

ARTICLE

Received 18 Mar 2015 | Accepted 5 Jun 2015 | Published 22 Jul 2015

DOI: 10.1038/ncomms8749

OPEN

Patterned arrays of lateral heterojunctions within monolayer two-dimensional semiconductors

Masoud Mahjour-Samani¹, Ming-Wei Lin¹, Kai Wang¹, Andrew R. Lupini², Jaekwang Lee¹, Leonardo Basile^{1,3}, Abdelaziz Boulesbaa¹, Christopher M. Rouleau¹, Alexander A. Puretzy¹, Iliia N. Ivanov¹, Kai Xiao¹, Mina Yoon¹ & David B. Geohegan¹

The formation of semiconductor heterojunctions and their high-density integration are foundations of modern electronics and optoelectronics. To enable two-dimensional crystalline semiconductors as building blocks in next-generation electronics, developing methods to deterministically form lateral heterojunctions is crucial. Here we demonstrate an approach for the formation of lithographically patterned arrays of lateral semiconducting heterojunctions within a single two-dimensional crystal. Electron beam lithography is used to pattern MoSe₂ monolayer crystals with SiO₂, and the exposed locations are selectively and totally converted to MoS₂ using pulsed laser vaporization of sulfur to form MoSe₂/MoS₂ heterojunctions in predefined patterns. The junctions and conversion process are studied by Raman and photoluminescence spectroscopy, atomically resolved scanning transmission electron microscopy and device characterization. This demonstration of lateral heterojunction arrays within a monolayer crystal is an essential step for the integration of two-dimensional semiconductor building blocks with different electronic and optoelectronic properties for high-density, ultrathin devices.

¹Center for Nanophase Materials Sciences, Oak Ridge National Laboratory, Oak Ridge, Tennessee 37831, USA. ²Materials Science and Technology Division, Oak Ridge National Laboratory, Oak Ridge, Tennessee 37831, USA. ³Departamento de Física, Escuela Politécnica Nacional, Quito 170525, Ecuador. Correspondence and requests for materials should be addressed to M.M.-S. (email: mahjourisamm@ornl.gov) or to D.B.G. (email: geohegandb@ornl.gov).

Two-dimensional (2D) layered semiconductors^{1,2}, notably the transitional metal dichalcogenide (TMD) families (MX_2 : M = Mo, W, Nb; X = S, Se, Te)¹ in which M atoms are sandwiched between two planes of X atoms, have recently attracted significant attention due to their novel electronic and optoelectronic properties and potential applications for new generations of flexible field-effect transistors^{3,4}, photovoltaics⁵, light-emitting diodes⁶ and sensors⁷. High-quality mono- and few-layer samples for prototype devices have been synthesized via various techniques including mechanical cleavage⁸, chemical exfoliation^{9,10}, vapour phase transport^{11,12} and laser-based methods^{13,14}. However, the next challenge for 2D material-based ultrathin integrated circuits is the controllable formation of semiconductor heterojunctions, either by vertically stacking different layers or by formation of lateral heterojunctions of different semiconductors within a single layer^{15–17}. Lithographic patterning and compatible synthesis approaches are required for high-density integration of semiconductor heterojunctions, as was recently demonstrated for lateral graphene interconnects embedded within an insulating monolayer of boron nitride by etching and regrowth processes¹⁷. Alternatively, phase engineering of patterned regions of MoS_2 crystals by exposure to liquid *n*-butyl lithium has recently achieved the transformation from a semiconducting to a metallic, metastable phase within a single layer⁴.

The most commonly explored method for the formation of a single heterojunction is vapour transport growth (VTG), which has resulted in lateral and vertical epitaxy between semiconducting TMDs such as $\text{MoS}_2/\text{MoSe}_2$, $\text{MoSe}_2/\text{WSe}_2$ and MoS_2/WS_2 (refs 18–20). By alternating precursor vapours and adjusting the growth temperature, disparate materials can be nucleated and grown on the edges (lateral junctions) or on top (vertical junctions) of as-grown crystals. However, typical VTG involves well-known challenges of highly non-uniform spatial control over nucleation, growth and layer control, owing to poor understanding and control over gas flow dynamics, chemical reactions and boundary layer diffusion. So far, these challenges as well as contamination by reaction byproducts, and reactivity at exposed crystal edges have limited the scalable and controllable formation of patterned heterojunctions between TMDs by this route.

Here we demonstrate the formation of patterned arrays of lateral heterojunctions between 2D layered semiconductors, $\text{MoSe}_2/\text{MoS}_2$, within the confines of a single monolayer MoSe_2 crystal. Heterojunction arrays are formed by sulfur replacement of Se (refs 21,22) within MoSe_2 (lattice constant 3.288 Å, optical bandgap 1.55 eV)^{19,23}, converting it to MoS_2 (lattice constant

3.160 Å, optical bandgap 1.85 eV)^{24,25} in predefined locations. Using well-developed and scalable photolithography and electron beam lithography processes, a variety of patterns exposed on monolayer MoSe_2 crystals are selectively converted to MoS_2 by pulsed laser vaporization of sulfur, producing predefined arrays of lateral $\text{MoSe}_2/\text{MoS}_2$ heterojunctions within a single monolayer. This process provides a unique capability for the digital delivery of a precise amount of sulfur atoms with super-thermal kinetic energies during the conversion process, allowing controllable sulfurization for either alloying or total conversion of MoSe_2 to MoS_2 . Raman and photoluminescence (PL) spectroscopy and mapping confirm the formation of periodic heterojunctions. High-angle annular dark-field atomic resolution scanning transmission electron microscopy (STEM) reveals that the MoS_2 is comparable in quality to pristine material, with sharp (~ 5 nm) heterojunction boundaries. This controllable and versatile formation of lithographically patterned lateral heterojunction arrays offers the potential for their integration as 2D layer ‘building blocks’, along with metal/insulator domains, for next-generation electronics.

Results

Formation of patterned arrays of lateral heterojunctions.

Figure 1 schematically illustrates the experimental steps for the formation of periodic lateral heterojunctions. The starting monolayer MoSe_2 crystals with lateral sizes ranging from 10 to 100 μm were synthesized using a previously reported method^{11,13} (Supplementary Fig. 1; Supplementary Note 1). The crystals were then simply masked by conventional patterning processes, followed by selective conversion of the unmasked MoSe_2 to MoS_2 by pulsed laser vaporization of sulfur. The masking material (~ 50 nm SiO_2) was electron beam evaporated and was found to be quite effective in protecting the areas of the 2D crystal underneath from sulfurization.

Prior to the patterning process and formation of heterojunction arrays, the conversion of 2D monolayers was studied at various temperatures for different numbers of sulfur pulses to understand and optimize the process (Supplementary Note 2). PL and Raman spectroscopies were used to investigate the crystal conversion process at various conditions and to reveal their optical properties (Supplementary Fig. 2). We found that MoSe_2 nanosheets are totally converted to MoS_2 for substrate temperatures above 600 °C and 300 laser-vaporized sulfur pulses, whereas temperatures and laser pulses below 600 °C and 300 pulses, respectively, resulted in the formation of intermediate compositions. At temperatures above 800 °C, decomposition and

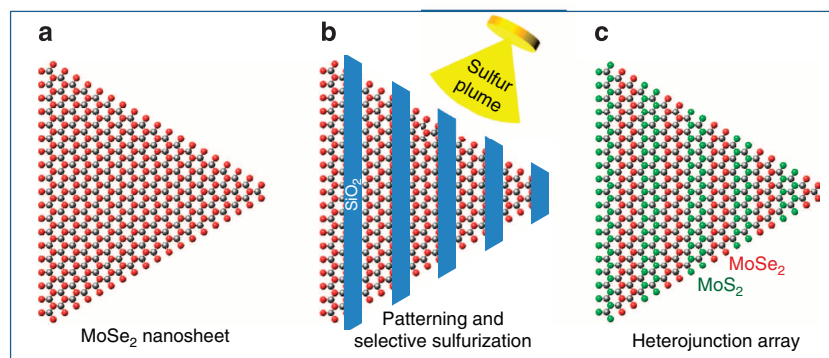


Figure 1 | Schematic illustration of the experimental steps for the formation of $\text{MoSe}_2/\text{MoS}_2$ heterojunction arrays. (a) Starting MoSe_2 monolayer crystal. (b) MoSe_2 is patterned by e-beam lithography and SiO_2 deposition, followed by sulfurization of uncovered areas. The SiO_2 mask is used to prevent the underlying MoSe_2 regions from reacting with sulfur while the exposed regions are converted to MoS_2 . (c) Formation of arrays of lateral $\text{MoSe}_2/\text{MoS}_2$ heterojunctions within the monolayer crystal.

damage of the crystals occurred. Therefore, substrate temperatures were fixed at 700 °C with 400 sulfur pulses to ensure a complete conversion of MoSe₂ to MoS₂. Conversion of WSe₂ to WS₂ was also achieved by the same process (Supplementary Fig. 3; Supplementary Note 3) to demonstrate the broad applicability and advantages of the technique.

The thermodynamic stability and optical bandgaps of various 2D transition metal dichalcogenide alloys (MX₂(1-x)X'_{2x} where M=Mo, W and X, X'=S, Se, Te) have previously been computationally predicted to understand the mixing and phase-segregation behaviour for different alloy compositions^{26,27}. Of these, MoS₂xSe₂(1-x) alloys were found to have the lowest free energy of mixing^{26,27}, yet all MX₂(1-x)X'_{2x} were predicted to form stable alloys with complete miscibility at the moderate temperatures typically employed during chemical vapour deposition or bulk synthesis, and with continuously tunable direct bandgaps, making them good candidates for 2D optoelectronics²⁶.

Spectroscopic characteristics of heterojunctions. Raman and PL spectroscopy were used to probe the structures spatially, monitor the conversion degree and to map the heterojunction arrays within the monolayer crystals. Figure 2a,b shows optical and atomic force microscopy images of a typical MoSe₂ 2D crystal. The corresponding Raman maps of the crystal before and after the full conversion process are shown in Fig. 2c,d. The MoSe₂ and MoS₂ Raman maps are plotted for the E_{2g}¹ mode of MoSe₂ at 238 cm⁻¹ and E_{2g}¹ modes of MoS₂ at 403 cm⁻¹, respectively^{10,13}. Representative Raman and PL spectra of the flake before and after the conversion process are shown in Fig. 2e,f, indicating MoSe₂ and MoS₂ Raman peaks similar

to those reported in the literature^{10,13}. The uniform intensity distribution in the Raman maps indicates spatial uniformity of the 2D crystals both before and after the conversion. Figure 2g,h shows the formation of various lateral heterojunction arrays prepared by our patterning and selective conversion process. Similarly, the uniform intensity of Raman maps clearly indicates the spatial uniformity of the MoSe₂ and MoS₂ domains, and formation of heterojunction arrays within the monolayer crystals. The Raman and PL spectra obtained from the pristine and converted regions of the crystals are similar to the ones shown in Fig. 2e,f.

STEM characterization of heterojunctions. Crystalline structures of the converted and pristine regions as well as their heterojunction boundaries were also studied by atomic resolution Z-contrast STEM. Figure 3a,b shows the optical image and corresponding Raman map of a typical patterned/converted layer transferred onto a grid for STEM imaging (Supplementary Fig. 4; Supplementary Note 4). As shown in Fig. 3c, atomic resolution Z-contrast STEM images are taken at the heterojunction that clearly shows both MoSe₂ (Fig. 3d) and MoS₂ (Fig. 3e) 2D crystal domains. The line and surface intensity profiles of the selected regions in Fig. 3c are shown in Fig. 3f,g. Likewise, Fig. 3h,i shows a STEM image of a boundary with its corresponding electron energy loss spectroscopy map showing the sulfur content (in green) as a function of position. It is clear that both pristine MoSe₂ and converted MoS₂ regions lie within the same honeycomb lattice with no grain boundaries—that is, the MoSe₂ crystal serves as a template, maintaining the same crystal orientations throughout the whole structure. As can be seen from the STEM image, the interface has a finite width similar to that reported for

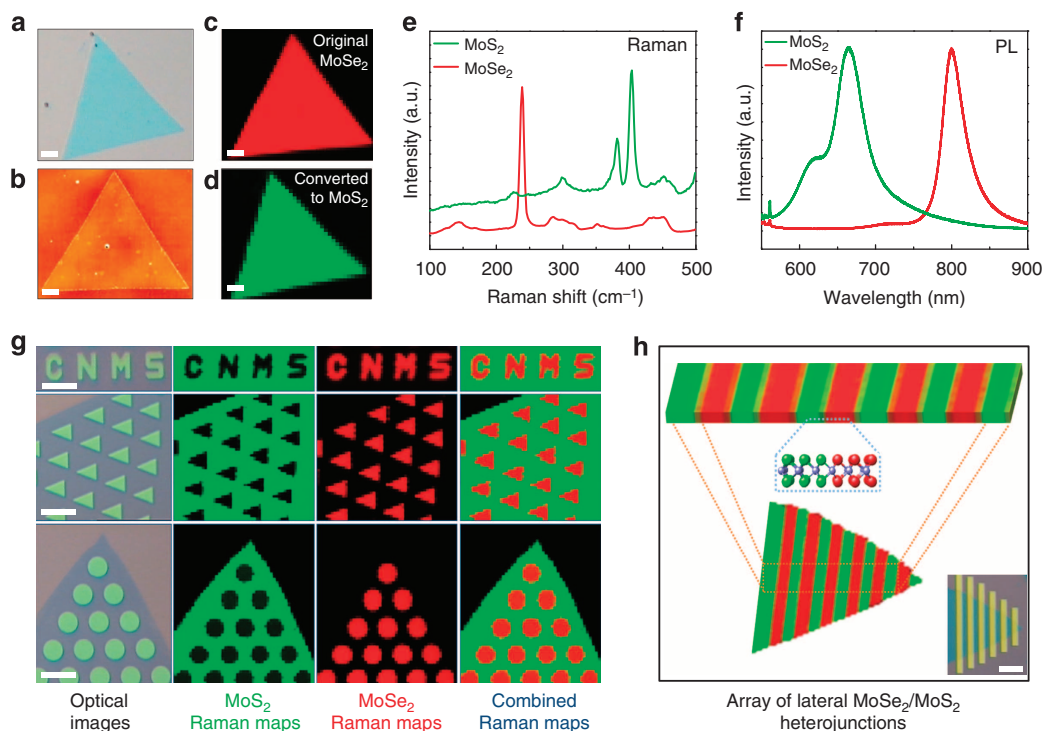


Figure 2 | Conversion of MoSe₂ to MoS₂ and the formation of lateral heterojunction arrays. (a,b) Optical and atomic force microscopy images of a typical MoSe₂ monolayer with a lateral size of ~40 μm. (c,d) Raman maps of a monolayer nanosheet before and after the complete conversion process (400 pulses at 700 °C), respectively, indicating uniform intensity across the entire crystal. (e,f) Representative Raman and PL spectra of the pristine MoSe₂ and converted MoS₂ regions. (g,h) Various examples of lateral heterojunction arrays formed within monolayer crystals by patterning and selective conversion processes. The green, red and combined Raman maps are obtained from corresponding optical images, representing the MoS₂ (intensity map at 403 cm⁻¹), MoSe₂ (intensity map at 238 cm⁻¹) and overlaid MoSe₂/MoS₂ regions, respectively. Scale bars, 5 μm.

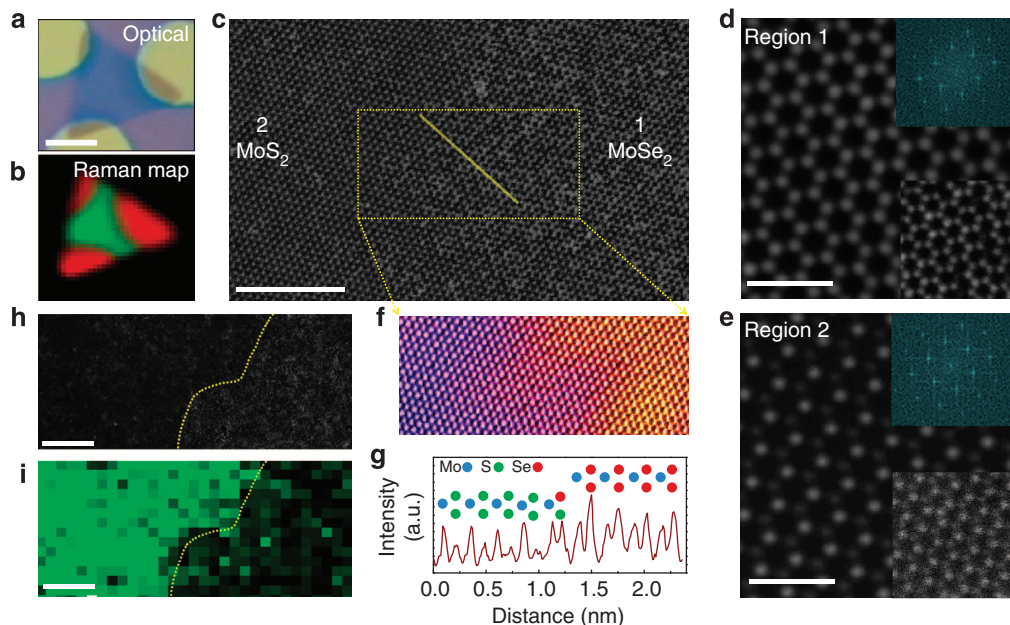


Figure 3 | STEM Z-contrast image and elemental imaging of a heterojunction. (a,b) Optical image and corresponding Raman map of a patterned nanosheet on a SiO_2 substrate (scale bar, $5\ \mu\text{m}$). The SiO_2 masks (circular discs in a) are removed during KOH etching, and the transfer of the nanosheet onto the TEM grids. (c) Low-magnification Z-contrast image of the nanosheet showing the MoSe_2 and MoS_2 regions with a finite boundary across the domains (scale bars, $5\ \text{nm}$). (d,e) Fourier filtered images of the atomic resolution Z-contrast images of the MoSe_2 and MoS_2 (bottom insets in the images) domains with corresponding fast Fourier transform patterns (top insets in the images). (f,g) Surface and line intensity profiles of the squared and line-marked regions in c. (h,i) Low-magnification image of a boundary with its corresponding electron energy loss spectroscopy map showing the sulfur concentration (scale bars, $5\ \text{nm}$).

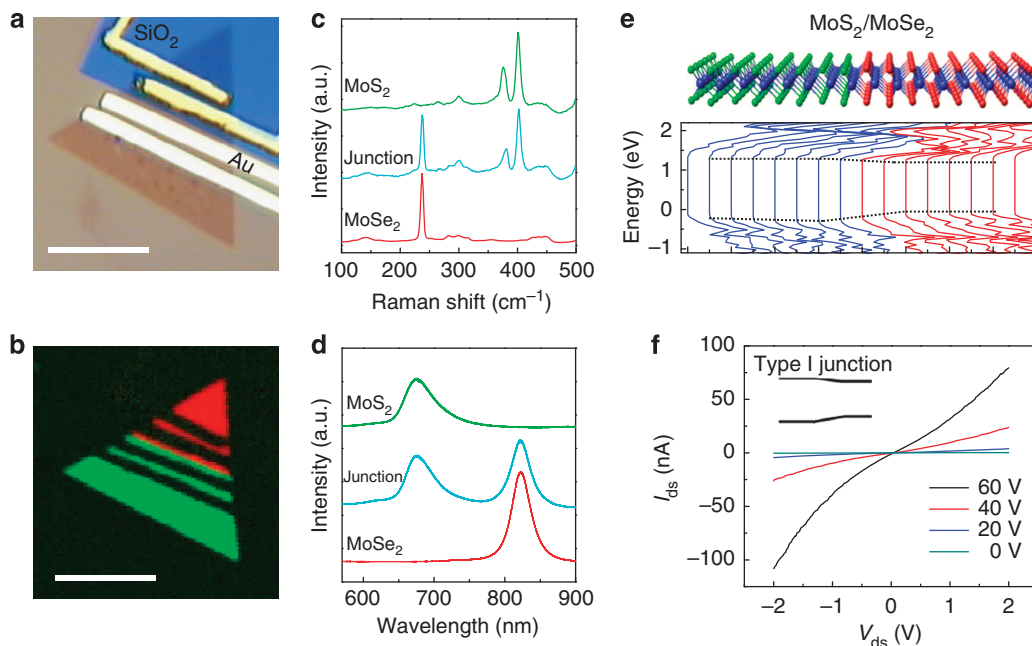


Figure 4 | Electrical transport properties. (a,b) Optical and Raman map of a $\text{MoS}_2/\text{MoSe}_2$ (green/red) heterojunction device. (c,d) Raman and PL spectra of MoS_2 and MoSe_2 obtained from each region showing a distinct peak for regions away from the junction and appearance of both peaks at the junction. (e) First-principles DFT calculation of MoSe_2 and MoS_2 superlattices showing the formation of type-I band alignment. (f) $I_{\text{ds}} - V_{\text{ds}}$ characteristics of the heterojunction showing an n-n junction behaviour at the interface.

$\text{MoSe}_2/\text{WSe}_2$ heterojunctions¹⁹. The boundary appears to be a $\text{MoS}_x\text{Se}_{1-x}$ ternary alloy with a composition gradient over a distance of several nanometres. The sharpness of the heterojunctions is related to the e-beam lithography and patterning processes used in this work, which can be improved further.

Electrical transport properties. The electrical transport properties of pristine MoSe_2 , converted MoS_2 and their heterojunctions were studied by forming a device structure. Figure 4a shows an example of a device structure fabricated in this work. Prior to the conversion process, two electrodes were fabricated on one side of

the crystal to measure the transport properties of the pristine MoSe₂. Then, this part was covered with a SiO₂ mask and the sulfurization was carried out, resulting in the conversion of the exposed half of the crystal to MoS₂. Two electrodes were then fabricated on this half to measure the electrical transport characteristics of the converted MoS₂ region. Figure 4b shows the Raman map of the device with red and green colours clearly indicating the MoSe₂ and MoS₂ regions, respectively, and their boundaries. Representative Raman and PL spectra of these regions are also shown in Fig. 4c,d, indicating distinct Raman and PL peaks for each domain while observing simultaneous MoSe₂ and MoS₂ peaks right at the junction.

To understand band alignment at the interface, first-principles calculations, based on density functional theory, were performed using the Vienna *ab initio* Simulation Package (Supplementary Note 5). As illustrated in Fig. 4e, we considered a supercell in which eight zigzag rows of MoS₂ joined eight rows of MoSe₂, and plotted the partial density of states projected onto the atomic rows in the MoS₂ and MoSe₂ across the heterojunction. From the projected density of states, we can see that there exists an obvious graded bandgap across the heterojunction. In particular, we find that the lateral MoS₂/MoSe₂ heterojunction forms a type-I band alignment, as indicated by the dotted line (Fig. 4e), since the bandgap of MoS₂ entirely overlaps that of MoSe₂.

$I_{ds} - V_{ds}$ curves were obtained from pristine MoSe₂, converted MoS₂ and their heterojunction to investigate their transport characteristics. According to the measured $I_{ds} - V_{ds}$ curves, both MoSe₂ and converted MoS₂ show n-type behaviour (Supplementary Fig. 5) similar to the previously reported work^{11,12}. Consequently, as shown in Fig. 4f, their boundary shows transport characteristic of an n-n heterojunction. The smaller current amplitude across the heterojunction boundary may be attributed to electron scattering at the heterojunction and the type of their band alignment.

Discussion

In conclusion, through lithographic patterning and controllable conversion of MoSe₂ to MoS₂, arrays of lateral MoSe₂/MoS₂ heterojunctions have been synthesized within a monolayer 2D crystal. Electron beam lithography coupled with vacuum deposition of SiO₂ masks and sulfur, two scalable techniques used in the semiconductor industry, were employed to form sharp (~5 nm) heterojunctions comparable to those formed by heteroepitaxy, without the non-uniformities typically introduced in VTG processes. Pulsed laser vaporization provided a controllable and rapid method to explore the conversion dynamics through the digital delivery of precise quantities of the sulfur precursor. The patterning and selective conversion process demonstrated here for semiconductor heterojunctions appears to be a powerful technique that could be extended to form other metallic, insulating and semiconducting regions within 2D materials required for ultrathin electronics.

Methods

E-beam patterning process. Electron beam lithography (FEI DB-FIB with Raith pattern writing software) was used for MoSe₂/MoS₂ heterostructure device fabrication. First, a layer of PMMA 495A4 was spin-coated on top of the MoSe₂ flakes, followed by a 180°C bake on a hot plate. After pattern writing and developing, 50 nm of SiO₂ was deposited using electron beam evaporation to serve as conversion masks. For device fabrication, 5 nm of Ti and 30 nm of Au were deposited using electron beam evaporation to serve as electrodes on the MoSe₂ flakes. After the MoSe₂ was converted to MoS₂, electron beam lithography was conducted again to place electrodes on the MoS₂. Finally, lift-off using acetone/IPA was used to reveal well-defined electrodes on both the MoSe₂ and converted MoS₂ flakes.

Conversion process. The conversion was performed in a vacuum (~10⁻⁵ Torr) chamber where a forward directed laser-vaporized sulfur plume was generated and digitally delivered to the surface of the crystals²⁸. The vaporization target was prepared by compressing sulfur powder (99%, Sigma-Aldrich) into a pellet, and the laser fluence was adjusted to about 0.5 J cm⁻² (spot size of 2 × 5 mm and repetition rate of 0.5 Hz) to ensure the transfer of a fixed amount of sulfur onto the crystals for all of the experimental conditions. The conversion was conducted under various substrate temperatures and laser pulses to understand and optimize the process (Supplementary Fig. 2; Supplementary Note 2).

Optical characterizations. Raman and PL mapping and spectroscopy were performed in a Renishaw inVia micro-Raman system using a 532-nm laser excitation source, 1,800 g mm⁻² grating and a laser power of about 1–5 mW through × 50 and × 100 objective lenses at room temperature. Maps were obtained with step sizes ranging from 0.3 to 1 μm. WiRE software was used to analyse and plot the maps for individual MoSe₂/MoS₂ sections and their overlaid images.

STEM Z-contrast imaging and analysis. All STEM samples were baked at 160 °C for 8 h under vacuum before the microscopy experiment. STEM imaging was performed on an aberration-corrected Nion UltraSTEM-100 operating at 60 kV. The convergence semi-angle for the incident probe was 31 mrad. Z-contrast images were gathered for a half-angle range of ~86–200 mrad. Electron energy loss spectroscopy and spectrum imaging was performed using a Gatan Enfina with a nominal collection angle of 35 mrad.

Electrical transport characterization. The electrical measurement of MoSe₂/MoS₂ field-effect transistor devices was conducted in a vacuum chamber (~10⁻⁶ Torr) using a Keithley 4200 semiconductor analyzer. The drain/source voltage (V_{ds}) was set at 2 V with a gate voltage that swept from -60 to +60 V for transport measurement.

References

- Chhowalla, M. *et al.* The chemistry of two-dimensional layered transition metal dichalcogenide nanosheets. *Nat. Chem.* **5**, 263–275 (2013).
- Butler, S. Z. *et al.* Progress, challenges, and opportunities in two-dimensional materials beyond graphene. *ACS Nano* **7**, 2898–2926 (2013).
- Pradhan, N. R. *et al.* Ambipolar molybdenum diselenide field-effect transistors: field-effect and hall mobilities. *ACS Nano* **8**, 7923–7929 (2014).
- Kappera, R. *et al.* Phase-engineered low-resistance contacts for ultrathin MoS₂ transistors. *Nat. Mater.* **13**, 1128–1134 (2014).
- Tsai, M. L. *et al.* Monolayer MoS₂ heterojunction solar cells. *ACS Nano* **8**, 8317–8322 (2014).
- Sundaram, R. S. *et al.* Electroluminescence in single layer MoS₂. *Nano Lett.* **13**, 1416–1421 (2013).
- Perkins, F. K. *et al.* Chemical vapor sensing with monolayer MoS₂. *Nano Lett.* **13**, 668–673 (2013).
- Li, H., Wu, J. M. T., Yin, Z. Y. & Zhang, H. Preparation and applications of mechanically exfoliated single-layer and multi layer MoS₂ and WSe₂ nanosheets. *Acc. Chem. Res.* **47**, 1067–1075 (2014).
- Coleman, J. N. *et al.* Two-dimensional nanosheets produced by liquid exfoliation of layered materials. *Science* **331**, 568–571 (2011).
- Zheng, J. *et al.* High yield exfoliation of two-dimensional chalcogenides using sodium naphthalenide. *Nat. Commun.* **5**, 2995 (2014).
- Wang, X. *et al.* Chemical vapor deposition growth of crystalline monolayer MoSe₂. *ACS Nano* **8**, 5125–5131 (2014).
- Najmaei, S. *et al.* Vapour phase growth and grain boundary structure of molybdenum disulphide atomic layers. *Nat. Mater.* **12**, 754–759 (2013).
- Mahjouri-Samani, M. *et al.* Digital transfer growth of patterned 2D metal chalcogenides by confined nanoparticle evaporation. *ACS Nano* **8**, 11567–11575 (2014).
- Mahjouri-Samani, M. *et al.* Pulsed laser deposition of photoresponsive two-dimensional GaSe nanosheet networks. *Adv. Funct. Mater.* **24**, 6365–6371 (2014).
- Zeng, Q. *et al.* Band engineering for novel two-dimensional atomic layers. *Small* **11**, 1868–1884 (2014).
- Duesberg, G. S. Heterojunctions in 2d semiconductors a perfect match. *Nat. Mater.* **13**, 1075–1076 (2014).
- Levendorf, M. P. *et al.* Graphene and boron nitride lateral heterostructures for atomically thin circuitry. *Nature* **488**, 627–632 (2012).
- Duan, X. *et al.* Lateral epitaxial growth of two-dimensional layered semiconductor heterojunctions. *Nat. Nanotechnol.* **9**, 1024–1030 (2014).
- Huang, C. *et al.* Lateral heterojunctions within monolayer MoSe₂-WSe₂ semiconductors. *Nat. Mater.* **13**, 1096–1101 (2014).
- Gong, Y. *et al.* Vertical and in-plane heterostructures from WS₂/MoS₂ monolayers. *Nat. Mater.* **13**, 1135–1142 (2014).
- Su, S.-H. *et al.* Controllable synthesis of band gap-tunable and monolayer transition metal dichalcogenide alloys. *Front. Energy Res.* **2**, 1–5 (2014).

22. Li, H. *et al.* Growth of alloy $\text{MoS}_{(2-x)}\text{Se}_2(1-x)$ nanosheets with fully tunable chemical compositions and optical properties. *J. Am. Chem. Soc.* **136**, 3756–3759 (2014).
23. James, P. B. & Lavik, M. T. Crystal structure of MoSe_2 . *Acta Crystallogr.* **16**, 1183 (1963).
24. Young, P. A. Lattice parameter measurements on molybdenum disulfide. *J. Phys. D Appl. Phys.* **1**, 936 (1968).
25. Nayak, A. P. *et al.* Pressure-dependent optical and vibrational properties of monolayer molybdenum disulfide. *Nano Lett.* **15**, 346–353 (2015).
26. Kang, J., Tongay, S., Li, J. B. & Wu, J. Q. Monolayer semiconducting transition metal dichalcogenide alloys: stability and band bowing. *J. Appl. Phys.* **113**, 143703 (2013).
27. Komsa, H. P. & Krashennikov, A. V. Two-dimensional transition metal dichalcogenide alloys: stability and electronic properties. *J. Phys. Chem. Lett.* **3**, 3652–3656 (2012).
28. Lowndes, D. H., Geohegan, D. B., Puzos, A. A., Norton, D. P. & Rouleau, C. M. Synthesis of novel thin-film materials by pulsed laser deposition. *Science* **273**, 898–903 (1996).

Acknowledgements

Synthesis science including crystal growth, *in situ* plume diagnostics, TEM analysis, SEM and AFM studies and conversion technique development (M.M.-S., K.W., J.L., A.R.L., K.X., D.B.G., C.M.R., A.A.P. and M.Y.) was supported by the US Department of Energy, Office of Science, Basic Energy Sciences, Materials Sciences and Engineering Division and performed in part as a user project at the Center for Nanophase Materials Sciences, which is a DOE Office of the Science User Facility. Characterization science at Center for Nanophase Materials Sciences (CNMS) including optical characterization and lithography techniques (M.-W.L., A.B. and I.N.I.) was supported by the Scientific User Facilities Division. L.B. was supported by the National Secretariat of Higher Education, Science, Technology and Innovation of Ecuador (SENESCYT).

Author contributions

M.M.-S. designed and performed the synthesis and conversion experiments, and obtained Raman and PL data with I.N.I. M.-W.L. and K.X. participated in patterning, device fabrication and transport characterization. J.L. and M.Y. performed theoretical modelling. K.W. participated in the synthesis of MoSe_2 nanosheets. A.R.L. and L.B. carried out the STEM study and analysis. C.M.R., A.B., A.A.P. and D.B.G. participated in design study, data analysis, discussions and manuscript preparation. All the authors discussed the results and commented on the manuscript.

Additional information

Supplementary Information accompanies this paper at <http://www.nature.com/naturecommunications>

Competing financial interests: The authors declare no competing financial interests.

Reprints and permission information is available online at <http://npg.nature.com/reprintsandpermissions/>

How to cite this article: Mahjouri-Samani, M. *et al.* Patterned arrays of lateral heterojunctions within monolayer two-dimensional semiconductors. *Nat. Commun.* **6**:7749 doi: 10.1038/ncomms8749 (2015).



This work is licensed under a Creative Commons Attribution 4.0 International License. The images or other third party material in this article are included in the article's Creative Commons license, unless indicated otherwise in the credit line; if the material is not included under the Creative Commons license, users will need to obtain permission from the license holder to reproduce the material. To view a copy of this license, visit <http://creativecommons.org/licenses/by/4.0/>